

# Probabilistic prediction of the time to hard freeze using seasonal weather forecasts and survival time methods

Thea Roksvåg<sup>\*1</sup>, Alex Lenkoski<sup>1</sup>, Michael Scheuerer<sup>1</sup>, Claudio Heinrich-Mertsching<sup>1</sup>,  
and Thordis L. Thorarinsdottir<sup>1</sup>

<sup>1</sup>Norwegian Computing Center, Postboks 114, 0314 Blindern, Oslo, Norway

January 5, 2022

## Abstract

Agricultural food production and natural ecological systems depend on a range of seasonal climate indicators that describe seasonal patterns in climatological conditions. This paper proposes a probabilistic forecasting framework for predicting the end of the freeze-free season, or the time to a mean daily near-surface air temperature below 0 °C (here referred to as hard freeze). The forecasting framework is based on the multi-model seasonal forecast ensemble provided by the Copernicus Climate Data Store and uses techniques from survival analysis for time-to-event data. The original mean daily temperature forecasts are statistically post-processed with a mean and variance correction of each model system before the time-to-event forecast is constructed. In a case study for a region in Fennoscandia covering Norway for the period 1993-2020, the proposed forecasts are found to outperform a climatology forecast from an observation-based data product at locations where the average predicted time to hard freeze is less than 40 days after the initialization date of the forecast on October 1.

## 1 Introduction

Agricultural decisions such as planting, harvest timing and field fertilization, are in large steered by weather and climate conditions, including conditions on subseasonal to seasonal timescales. For surface air temperature, the relevant seasonal climate indicators, or agroclimatic indicators, are mainly related to heat accumulation and frost characteristics. The most common index for heat accumulation is usually referred to as growing degree days, while frost characteristics are described by the onset, end, and duration of the freeze-free season for various freezing thresholds (Kukul and Irmak, 2018; Weltzin et al., 2020). Skillful predictions of these agroclimatic indicators are needed for both agricultural operations planning and for predicting crop growth and yield potential, especially in the light of worldwide observed changes in the indicators over time due to climate change (e.g. Kunkel et al., 2004; Schwartz et al., 2006; Liu et al., 2008; Zhang et al., 2014).

Seasonal forecast users in the agricultural sector have criticized available forecasting products for a lack of forecast skill and usability. In particular, they have requested derived forecast products that directly predict relevant agroclimatic indicators, information on uncertainty and comparisons to previous years, see Klemm and McPherson (2017) and references therein. This contrasts current practice in subseasonal and seasonal forecasting to aggregate variables such as temperature and precipitation over months, seasons and/or spatial regions in order to achieve skill that outperforms climatological reference forecasts (e.g. Hemri et al., 2020; van Straaten et al., 2020).

Seasonal predictions of agroclimatic indicators are currently lacking and available seasonal information is commonly in the form of local or regional climatological information, see e.g. Angel et al. (2017). Similarly, approaches to predict agricultural outcomes on the seasonal scale, e.g. agricultural yield prediction, are not based on seasonal predictions of relevant agroclimatic indicators. Rather, predictions are often based on seasonal predictions for large-scale climate drivers such as the El Niño Southern Oscillation (Hammer et al., 1996; An-Vo et al., 2019; Lehmann et al., 2020). While such approaches work well in regions where the seasonal climate is heavily influenced by teleconnections, they may not generalize to

---

<sup>\*</sup>roksvag@nr.no

other regions. In a perspective, Fischer and Connor (2018) identify improved seasonal weather forecasts as a potential key factor for crop agronomy developments in the coming decades.

In this paper, we investigate the potential of seasonal forecasts to skillfully predict an agroclimatic indicator for the end of the freeze-free season. Specifically, we aim to predict the time to the next occurrence of hard freeze from the initialization date of the forecast, where hard freeze refers to a mean daily near-surface air temperature below 0°C. Using methods from survival analysis, a branch of statistics for analyzing the expected duration of time until an event occurs (Kalbfleisch and Prentice, 2011), we construct a probabilistic time-to-event forecast for the time to hard freeze based on a multi-model ensemble of seasonal temperature forecasts available from the Copernicus Climate Data Store (CDS). As suggested by e.g. Hemri et al. (2020) in the context of seasonal mean forecasts, the daily temperature forecasts are statistically post-processed to remove systematic biases and errors in the ensemble spread before they are processed further to construct the time-to-event forecast. The proposed methodology is applied to seasonal temperature forecasts for a region in Fennoscandia covering Norway for the period 1993-2020, where forecasts initialized on October 1 are used to predict time to hard freeze in the period October 1 to December 31.

While survival time analysis is a broad statistical field, such methods are rarely used in meteorology. We believe that this approach has great potential for use in a wide range of applications, including the modeling of the onset of the rainy season, or the time to the next drought. The current study forms an entry point showing how this theory can be combined with numerical weather predictions to provide probabilistic forecasts for the time to a specific event.

The remainder of the paper is organized as follows. The raw seasonal forecasts and the observation-based gridded data product used in the analysis are described in Section 2. The proposed statistical post-processing and survival analysis methods are described in Section 3, followed by a description of forecast evaluation approaches in Section 4. The results of the time to freeze forecasting are presented in Section 5, with conclusions and a discussion given in Section 6.

## 2 Data products

The time to frost forecasts proposed in this article are constructed based on seasonal subdaily near-surface air temperature forecasts from the Copernicus Climate Data Store (CDS). CDS provides a selection of seasonal forecast products from different weather centers around the globe<sup>1</sup>. The seasonal forecasts are generated by predicting the change in slow-varying components of the earth system, such as the ocean temperature. Based on the current state of the system and the directed movements of large ocean currents, it is possible to predict both ocean and atmospheric temperature several weeks or months ahead using numerical weather prediction models (NWP; Robertson and Vitart, 2018). The resulting forecasts are given as an ensemble, where each ensemble member represents one possible future weather scenario. As there are complex, non-linear interactions at play, forecasts at long lead times are associated with large uncertainty. At the typical seasonal lead times of one to three months, skillful forecasts can often only be obtained after considering monthly or weekly averages, often additionally averaged over large spatial regions (van Straaten et al., 2020).

We derive probabilistic forecasts for the time to hard freeze from NWP ensemble predictions with initialization date of October 1. October 1st was chosen since the first hard freeze typically occurs 0-3 months after this date within our study region in Fennoscandia, see Figure 1a. On the CDS, hindcasts with initialization date of October 1 were, at the time we downloaded the data, available for four NWP systems for a total of approximately 100 ensemble members. The four centres that produce these forecasts are the European Centre for Medium-Range Weather Forecasts (ECMWF), the Euro-Mediterranean Center for Climate Change (CMCC), Météo France and the UK Met Office. For 1993-2016 and 2020, hindcasts with 6 hour temporal resolution and lead times from 0 to 5-7 months were available for all four systems. For 2017-2019, only hindcasts from ECMWF were available. See Table 1 for further information on each NWP system and the data availability.

As Table 1 shows, the NWP forecasts are all delivered on a  $1 \times 1^\circ$  grid, but the grid specification varies between the systems. While the ECMWF forecasts are given on a grid centered at full-degree longitudes and latitudes ( $1^\circ$ ,  $2^\circ$ ,...), the remaining forecasts are on a grid shifted by half a degree ( $0.5^\circ$ ,  $1.5^\circ$ ,  $2.5^\circ$ ,...). Following the practice on the CDS website for monthly forecasts, we use a nearest neighbor

<sup>1</sup><https://confluence.ecmwf.int/display/CKB/C3S+Seasonal+Forecasts%3A+datasets+documentation>

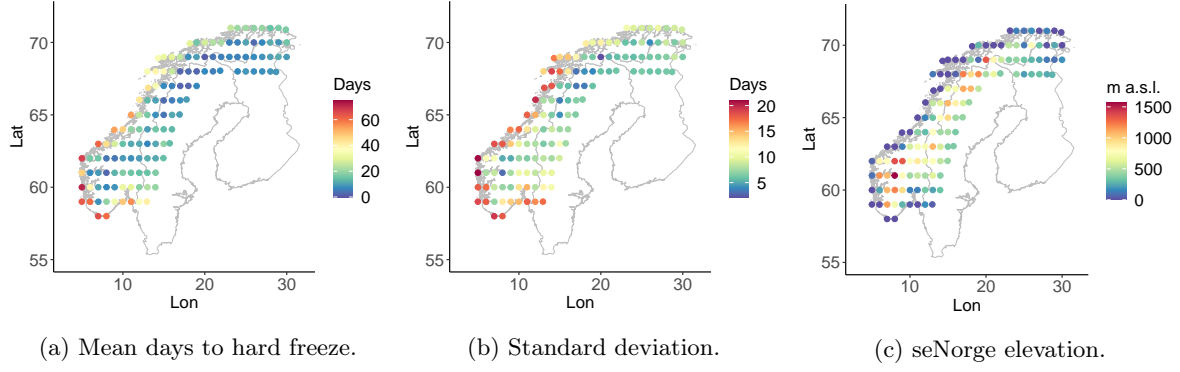


Figure 1: Mean number of days to hard freeze, from October 1st, for 1993-2020 for the seNorge product (left), the corresponding standard deviation (center) and seNorge’s model elevation in meters above sea level (right). The study locations are in Norway, Sweden, Finland and Russia, on an approximate  $1 \times 1^\circ$  grid.

approach to place the half degree products on the nearest full degree. This is assumed to be a reasonable approximation for our application, as the forecasts for each system is post-processed to reduce system specific, systematic errors. Furthermore, we consider mean daily temperatures when we derive the time to hard freeze forecasts. These are obtained by averaging the 6h subdaily temperature predictions for each forecast valid date.

Table 1: Information on the data products used in the analysis. The forecasts have initialization date of October 1st. The table shows the number of ensemble members the hindcasts for each of the systems have for most years. From 2017-2020 the ECMWF forecast has 51 ensemble members, while the CMCC and Météo France forecasts have 50 members in 2020. The UK Met Office forecast only has 2 ensemble members in 2020. The *Degrees* row indicates whether the forecasts are given for whole longitudes and latitudes ( $1^\circ$ ,  $2^\circ$ , ...) or half longitudes and latitudes ( $0.5^\circ$ ,  $1.5^\circ$ ,  $2.5^\circ$ , ...).

NWP system	ECMWF	CMCC	Météo France	UK Met Office	seNorge2018
Spatial resolution	$1^\circ \times 1^\circ$	$1^\circ \times 1^\circ$	$1^\circ \times 1^\circ$	$1^\circ \times 1^\circ$	1 km $\times$ 1 km
Degrees (half or whole)	Whole	Half	Half	Half	$\times$
Ensemble members	25	40	25	7	$\times$
Missing years	None	2017-2019	2017-2019	2017-2019	None

To validate and calibrate the seasonal forecasts, we use mean daily temperatures from the data product seNorge2018 for 1993-2020. The seNorge product is a gridded observation-based dataset developed at the Norwegian Meteorological Institute (MET Norway; Lussana et al., 2019) and freely available at <https://thredds.met.no/thredds/catalog/senorge/catalog.html>. It is derived from observations of temperature from 200-450 meteorological stations, depending on year. These are interpolated to a  $1 \times 1$  km grid covering the Norwegian mainland and parts of Sweden, Finland and Russia. The interpolation method is based on optimal interpolation (e.g. Gandin and Hardin, 1965; Kalnay, 2003), which is a data assimilation method where observations are combined with a background field. The background field is here an estimated temperature field based on how temperature varies with elevation, see Lussana et al. (2018, 2019) for details. The seNorge mean daily temperature dataset, and other seNorge products, have been used in a variety of studies (e.g. Erlandsen et al., 2021; Belušić et al., 2020; Handeland et al., 2021; Lawrence, 2020).

For agricultural applications, a hard freeze forecast is most useful if it provides information targeted towards a specific farm or field. In our experiments, we therefore aim to construct forecasts that predict the temperature locally at selected study locations that we can think of as farm locations. To select a set of locations we performed the following: Each whole longitude and latitude pair in the NWP grid was matched with the closest seNorge grid cell. Only NWP grid cells that were closer to a seNorge grid cell than 10 km were included in the analysis. This resulted in the 135 study locations shown in Figure 1a. For these, we computed the number of days to hard freeze from October 1 from the seNorge mean daily temperature data, where a day with hard freeze is defined here as a day with mean daily temperature below 0. The historical mean number of days to hard freeze for 1993-2020 is visualized in Figure 1a. The mean ranges from 1 to 72 days depending on distance from coast, elevation, longitude and latitude. In Figure 1b the corresponding standard deviation is presented, while the seNorge model elevation is shown

in Figure 1c for reference.

### 3 Predicting the time to hard freeze

#### 3.1 Post-processing daily NWP output

Numerical weather predictions are often subject to systematic biases. This is especially true for near-surface temperature forecasts over complex terrain, where differences between the model grid elevation and the true elevation (or, as in the present setting, the elevation associated with the seNorge product) entail systematic differences in the respective near-surface temperature climatologies (Dabernig et al., 2017; Keller et al., 2021). Statistical post-processing can remove these biases and thus lead to substantial improvements in forecast skill, even as NWP models continue to become better and their horizontal resolutions increase (Hemri et al., 2014). Methods proposed for the statistical post-processing of near-surface temperature forecasts range from basic, regression-based bias correction (Glahn and Lowry, 1972) over distributional regression methods, which also adjust the representation of uncertainty (e.g. Gneiting et al., 2005), to advanced machine learning techniques which permit the use of multiple predictors and/or non-linear predictor-predictand relationships (Messner et al., 2017; Taillardat et al., 2016; Rasp and Lerch, 2018; Roebber and Crockett, 2019).

Several applications require that the post-processed forecasts are provided in the form of an ensemble. This ensemble must not only be unbiased and represent the forecast uncertainty, but in addition it must also exhibit realistic co-variability across space and time. This is important for ensuring that predictions of spatially and/or temporally aggregated quantities such as areal means, minima/maxima over a certain time period, etc., also are calibrated. In the present application, correlations across forecast lead times are important since temperature forecasts which oscillate wildly over time can be expected to fall below a given temperature threshold sooner than a forecast that is more persistent over time, but has otherwise similar statistical characteristics. Unfortunately, most statistical post-processing techniques focus on the marginal forecast distributions and lose the multivariate information encompassed in the ensemble. Techniques to construct a full multivariate predictive distribution have been proposed in the literature (see Lerch et al. (2020) for a recent overview), but require additional modeling efforts. Alternatively, one can use methods like member-by-member post-processing approaches (Van Schaeybroeck and Vannitsem, 2015) which retain the rank correlation structure of the original ensemble forecasts. The post-processing approach used in the present study falls into this category as it adjust the members individually and leaves their temporal (and spatial) structure intact.

Let  $\mathcal{S}$  denote the study locations in Figure 1 and  $s \in \mathcal{S}$  a particular location. Further, let  $f_{s,t,y}^{k,m}$  be the mean daily temperature forecasted for day  $t$  after the forecast initialization date, for year  $y$ , NWP system  $k$ , ensemble member  $m$  and location  $s$ . We post-process the daily near surface air temperature forecasts in two steps. For each NWP system  $k$ , the forecasts are first standardized with respect to a system specific mean and standard deviation. The standardization is given by

$$\tilde{f}_{s,t,y}^{k,m} = \frac{(f_{s,t,y}^{k,m} - \tilde{\mu}_{s,t}^k)}{\tilde{\sigma}_{s,t}^k}, \quad (1)$$

where  $\tilde{\mu}_{s,t}^k$  is the mean daily temperature forecasted by system  $k$  for day  $t$  and location  $s$ , calculated based on historical ensemble members from this particular NWP system. Similarly,  $\tilde{\sigma}_{s,t}^k$  is the historical standard deviation for system  $k$ , day  $t$  and location  $s$ . In practice, when calculating  $\tilde{\mu}_{s,t}^k$  and  $\tilde{\sigma}_{s,t}^k$ , we leave out all members of the forecast corresponding to the current year  $y$ .

The next step is to re-standardize  $\tilde{f}_{s,t,y}^{k,m}$  with respect to historical observations from the target locations, in this case the seNorge locations in Figure 1. This is done as follows:

$$\hat{f}_{s,t,y}^{k,m} = \tilde{f}_{s,t,y}^{k,m} \cdot \hat{\sigma}_{s,t} + \hat{\mu}_{s,t}, \quad (2)$$

where  $\hat{\mu}_{s,t}$  is the mean observed daily temperature for location  $s$  on day  $t$ , and  $\hat{\sigma}_{s,t}$  is the corresponding observed standard deviation. When calculating  $\hat{\mu}_{s,t}$  and  $\hat{\sigma}_{s,t}$ , we leave out data from the current year  $y$  as these data are unobserved at the forecast time. The result of equations (1) and (2) is a post-processed ensemble  $\hat{f}_{s,t,y}^{k,m}$  where the mean and standard deviation of the marginal distribution of each member matches that of the observation for each target day and each target location.



This form of post-processing by recalibrating the model climatology is frequently used for seasonal weather forecasts (e.g. Weigel et al., 2009; Woldemeskel et al., 2018), and is similar in flavor to regression-based post-processing techniques. While regression-based techniques provide slightly more flexibility, Hemri et al. (2020) shows that they often perform poorly in related tasks in seasonal forecasting. This is a result of an increased risk of overfitting in the context of seasonal forecasts, where observed time series are short and the signal-to-noise ratio is small, see also Van Schaeybroeck and Vannitsem (2018) and Heinrich et al. (2021).

### 3.2 Time-to-event forecasts with survival analysis

We construct time to hard freeze forecasts by using methods from survival time analysis. In this subsection we provide a concise review of survival time modeling. This topic has a substantial literature associated with it and a number of texts deal with the study in detail, see e.g. Kalbfleisch and Prentice (2011) for a comprehensive introduction to the subject. While the methodology has become established in a diverse number of fields, it has gained most prominence in the field of biostatistics, where it is used to study the efficacy of treatments for disease, among other matters. A key aspect of the appeal of the survival time approach is that it can address a broad array of complications that arise when conducting real-world experiments, especially covariate-dependent censoring. Many of the complications encountered in medical studies are not present in our modeling and therefore we are able to specify a rather straightforward framework in this manuscript. Events other than the first hard freeze day could be considered with essentially no alteration to the framework, see Section 6.

Let  $\mathcal{T} = \{0, \dots, T\}$  denote a time sequence. In our study it is sufficient for  $\mathcal{T}$  to be discrete, but generalization to continuous time is straightforward. A survival time model  $\mathbb{S} : \mathcal{T} \rightarrow [0, 1]$  is a monotonically decreasing function where, for our purposes  $\mathbb{S}(0) = 1$  and  $\mathbb{S}(t) = p$  implies that at time  $t$ , there is a probability  $p$  that an event has occurred at some point in the interval  $(0, t]$ . In our hard freeze modeling  $\mathcal{T} = \{1, \dots, 92\}$  denotes the number of days from October 1 of a given year, and the event in question is the first day that the mean daily temperature is below 0. We here use  $\mathcal{T} = 92$ , corresponding to December 31, as our last possible hard freeze date.

In the survival time framework, an observation  $\mathbf{Y}_i$  consists of the pair  $\mathbf{Y}_i = (T_i, d_i)$ , where  $T_i \in \mathcal{T}$  is the observed time to the event or the last observed time of the process and  $d_i \in \{0, 1\}$  indicates whether or not the event occurred at  $T_i$ . In our example  $T_i$  is either the number of days after October 1 on which hard freeze first occurred (in which case  $d_i = 1$ ), or  $T_i = 92$  and  $d_i = 0$  indicating that hard freeze did not occur before December 31. See the attached files for example data.

Suppose we now have a collection of data  $\mathcal{D} = \{\mathbf{Y}_1, \dots, \mathbf{Y}_n\}$ . There exist a panoply of methods for estimating  $\mathbb{S}(t)$  using these data. The Kaplan-Meier (KM) estimator (Kaplan and Meier, 1958) is the classic nonparametric estimator of  $\mathbb{S}(t)$  and serves as the first step in any more detailed survival analysis. Let  $n_t = \sum_{i=1}^n \mathbf{1}\{T_i \geq t\}$  denote the number of observations still at risk (i.e. the event has not occurred yet) at time  $t$  and  $e_t = \sum_{i=1}^n \mathbf{1}\{T_i = t \cap d_i = 1\}$  denote the number of observations for which the event occurred at time  $t$ . The KM estimator models the probability that the event of interest has not yet occurred at time  $t$  and is formed as

$$\hat{\mathbb{S}}(t|\mathcal{D}) = \prod_{l=0}^t (1 - \lambda_l) \quad (3)$$

where

$$\lambda_l = e_l / n_l.$$

Let  $\mathbb{S}_{sy}(t)$  denote the year- $y$ -specific survival curve for a location  $s \in \mathcal{S}$ . In our study, we will compare three estimators of  $\mathbb{S}_{sy}(t)$ , all of which use the KM estimator (3) and differ solely on the basis of their input data. The estimator  $\hat{\mathbb{S}}(t|\mathcal{D}_{s,-y}^{seNorge})$  constructs  $\mathcal{D}$  from the seNorge data at  $s$  over the years 1993-2020, but excluding year  $y$  and serves as our leave-one-year-out hard freeze climatology. As such, we will write this as  $\hat{\mathbb{S}}_{sy}^C(t)$ . When calculating  $\hat{\mathbb{S}}_{sy}^C(t)$ , we have one data pair  $\mathbf{Y}_i = (T_i, d_i)$  per historical year. Each year is hence treated similarly as an individual in a classical survival analysis setting.

In addition to the climatology estimate, we consider two year-specific survival curves  $\hat{\mathbb{S}}(t|\mathcal{D}_{sy}^{Raw})$  and  $\hat{\mathbb{S}}(t|\mathcal{D}_{sy}^{Post})$  that represent our probabilistic time to hard freeze predictions for year  $y$ . In this case  $\mathcal{D}_{sy}^{Raw}$  is constructed from the raw ensemble forecast (or hindcast) for the year  $y$  initialized on October 1 for the ensemble systems discussed in Section 2.  $\mathcal{D}_{sy}^{Post}$  consist of the ensemble estimates after performing the

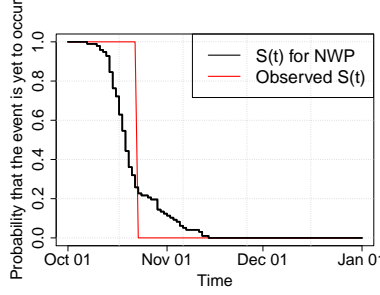


Figure 2: Example KM curve  $\hat{S}(t)$  for the time to hard freeze for a year and location based on the ensembles of several NWP systems (black). This is compared to the observed survival curve, which has probability 1 before hard freeze occurred historically for this year and location, and 0 afterwards.

post-processing according to Equation (2). For brevity we write these as  $\hat{S}_{sy}^R(t)$  and  $\hat{S}_{sy}^P(t)$ , respectively. When calculating  $\hat{S}_{sy}^R(t)$  and  $\hat{S}_{sy}^P(t)$ , we have one data pair  $\mathbf{Y}_i = (T_i, d_i)$  per ensemble member. Each ensemble member is hence treated similarly as an individual in a classical survival analysis setting.

In Figure 2, an example forecast  $\mathbb{S}_{sy}(t)$  for the time to hard freeze is shown. The uncertainty of the NWP ensemble is represented in an intuitive way through the shape of  $\mathbb{S}_{sy}(t)$  and how it decays over time. Each drop in  $\mathbb{S}_{sy}(t)$  corresponds to a time when at least one ensemble member experienced the first hard freeze after the forecast initialization date. When  $\hat{S}(t)$  is equal to 0, the event has occurred for all ensemble members before time  $t$ . If not all ensemble members predict hard freeze before the last day of the forecast, the  $\hat{S}(t)$  will simply not drop to zero.

## 4 Forecast evaluation

We construct time to hard freeze forecast,  $\hat{S}_{sy}^C(t)$ ,  $\hat{S}_{sy}^R(t)$  and  $\hat{S}_{sy}^P(t)$ , with initialization date October 1st for our 135 study locations and 28 years by using the methodology from Section 3. The time to freeze forecasts are evaluated under the paradigm that we aim to maximize the sharpness of the probabilistic forecasts subject to calibration (Gneiting et al., 2007). Calibration (or reliability) refers to the property that predicted probabilities match observed frequencies. Sharpness is a property of the prediction only, a sharper forecast being more informative about future events. To this aim, we apply rank histograms and proper scoring rules as described in the following two subsections.

In addition to evaluating time to hard freeze forecasts with initialization date of October 1, we evaluate survival curves for forecasts initialized on September 1. These are mainly used as a reference to the October forecasts to show how the forecast skill is affected when hard freeze occurs further into the future from the initialization date. The experimental set-up is otherwise identical to the one used for the October initializations.

### 4.1 Calibration assessment

Before evaluating the KM time-to-event forecasts, we perform a calibration assessment of the the post-processed ensembles. The goal is to explore whether post-processing of the coarse  $1 \times 1^\circ$  NWP forecasts results in calibrated daily mean temperature forecasts at the  $1 \times 1$  km scale and whether this translates into calibrated forecasts for the time to hard freeze. The calibration assessment is performed by calculating the rank of each seNorge observation within the corresponding forecast ensemble, and building rank histograms (Hamill, 2001). To facilitate comparison across forecast cases with varying ensemble size, we standardize the observed ranks to take values between 0 and 1 by subtracting 1 and then dividing by the ensemble size, with ties resolved at random (Heinrich, 2021).

For a calibrated forecast, the observed standardized ranks should be uniformly distributed on  $[0,1]$ . If the histogram is skewed to the left or right, it means that the ensemble underestimates or overestimates the quantity of interest. A  $\cup$ - or  $\cap$ -shaped histogram indicates under- or over-dispersion. In our study, we only have 28 years of data for each location. To increase our sample size, we calculate standardized ranks for the daily mean temperature for each location, for a group of lead times at once. Calibration

at all lead times in a group is thus evaluated simultaneously, and we wouldn't be able to tell whether e.g. an apparent bias applies to all or just a subset of those lead times. We summarize the resulting rank histograms by calculating the mean observed standardized ranks for each location. If the ensemble is unbiased, the mean should be close to 0.5. Smaller values of the mean observed standardized ranks indicate an overforecast bias, whereas values above 0.5 indicate an underforecast bias. We also compute the mean deviance from 0.5 for the observed standardized ranks. For a flat histogram we expect a value of 0.25. Smaller values indicate overdispersion of the forecast, whereas values above 0.25 indicate underdispersion, subject to the mean being close to 0.5.

We also consider rank histograms for our target variable, which is the predicted time to hard freeze. These can be derived in the same fashion as for the mean daily temperature. As the forecast and observations take discrete values between 1 and 92, we add random noise to the data to avoid ties when the observation rank within the ensemble is calculated. Furthermore, we cannot pool the observed ranks according to lead time here. Instead, we pool across all study locations, both for the raw and the post-processed ensemble forecasts.

## 4.2 Evaluating probabilistic time-to-event forecasts

To evaluate the KM predictions of time to hard freeze, the predicted survival curve  $\hat{S}_{sy}^R(t)$ ,  $\hat{S}_{sy}^P(t)$  or  $\hat{S}_{sy}^C(t)$  is compared to the observed survival curve  $S_{sy}^{obs}(t)$  for  $t = 1, 2, \dots, 92$  for the target locations. For year  $y$  and location  $s$ , the observed survival curve is 1 before frost occurred and 0 afterwards, see Figure 2 for an example.

For a fixed time  $t$ , a survival model simply issues a probabilistic forecast for a categorical event that takes either 0 or 1 as values, namely whether hard freeze has occurred up to the time  $t$  or not. Such predictions can be evaluated based on the average Brier score (Brier, 1950), which takes the form

$$BS_{s,M}(t) := \frac{1}{28} \sum_{y=1993}^{2020} (S_{sy}^{obs}(t) - \hat{S}_{sy}^M(t))^2,$$

where the model  $\hat{S}_{sy}^M$  is a placeholder for any of the models  $\hat{S}_{sy}^R$ ,  $\hat{S}_{sy}^P$  or  $\hat{S}_{sy}^C$  discussed in Section 2.3. We generally consider negatively oriented scores such that lower scores indicate better predictive performance.

The score  $BS_{s,M}(t)$  is a measure of the predictive skill solely focusing on the prediction of the occurrence of hard freeze up to time  $t$ . The overall fit of the survival curve at location  $s$  can be assessed by summing ('integrating') the Brier scores over  $t$ , see Mogensen et al. (2012),

$$IBS_{s,M} := \frac{1}{92} \sum_{t=1}^{92} \left( \frac{1}{28} \sum_{y=1993}^{2020} (S_{sy}^{obs}(t) - \hat{S}_{sy}^M(t))^2 \right), \quad (4)$$

where  $T = 92$  is the highest considered  $t$ . As a visual example, in Figure 2 the integrated Brier score would simply be the integrated squared difference between the two lines. The integrated Brier score is equivalent to the continuous ranked probability score (CRPS; Hersbach, 2000) for the time to hard freeze and thus a proper score.

A natural question for evaluating predictions is whether the forecast exhibits higher skill than a climatological forecast. To facilitate direct comparison, proper scores can be transformed into skill scores, see Wilks (2011). The integrated Brier skill score for model  $M$  at location  $s$  is defined as

$$IBSS_{s,M} := \frac{IBS_{s,C} - IBS_{s,M}}{IBS_{s,C}},$$

where  $IBS_{s,C}$  is the integrated Brier score of the climatological model  $\hat{S}_{sy}^C$ . Skill scores are positively oriented, such that higher values indicate better predictive performance. They are normalized in the sense that a perfect forecast achieves a skill score of 1, and a forecast with the same skill as climatology achieves a skill score of 0. Positive skill scores thus indicate better predictive performance than a climatological forecast.

Above, we define location-specific evaluation scores. A year-specific integrated Brier (skill) score for the whole study area can be obtained similarly, by averaging over locations instead of years.

## 5 Results

In this section we present the results from the time to hard freeze analysis. We start by presenting the results from the calibration assessment, before considering the predictive performance of the time-to-event forecasts.

### 5.1 Calibration assessment

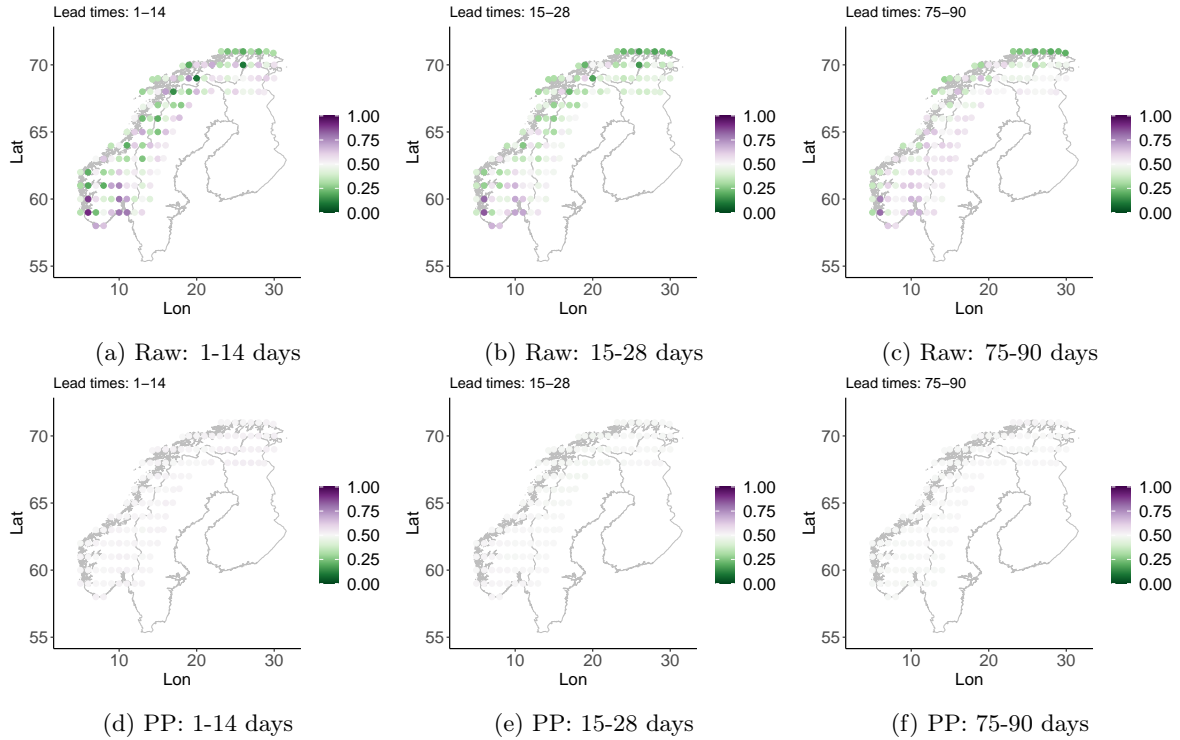


Figure 3: Mean observed standardized ranks for daily temperature forecasts initialized on October 1 for daily lead times 1-14 (leftmost column), 15-28 (middle column) and 75-90 (rightmost column) for the raw (top row) and the post-processed (bottom row) ensemble forecast. The results are aggregated over 1993-2020. If the forecast is calibrated, the mean observed standardized rank should be 0.5.

The mean observed standardized ranks for the daily temperature forecasts are shown in Figure 3 for some selected lead times for the raw and post-processed ensembles. Grid points colored in green indicate that the forecasts are too warm on average, whereas for purple grid points the forecasts are too cold on average. The results show that the raw ensemble is too warm at many grid points, in particular in the northern part of the study area and too cold at other grid points. We obtain a similar spatial distribution of mean ranks for all lead times, but the biases appear to be less extreme for the longest lead times (75-90 days). For the post-processed ensembles, the mean ranks are close to 0.5 for all study locations and lead times, indicating that the post-processed temperature forecasts are unbiased on average.

Figure 4a-4c show the mean rank deviation from 0.5, where a deviation of 0.25 indicates a calibrated forecast. While the values for the raw daily temperature forecast are mostly larger than 0.25, the biases seen in Figure 3 cause at least part of that increase and make it difficult to draw conclusions about additional dispersion errors in the ensemble. However, we can conclude from Figure 3 that the post-processed ensemble is unbiased and neither under- nor overdispersive. The post-processing algorithm hence seems to be able to translate a  $1 \times 1^\circ$  daily temperature forecast into a calibrated local temperature forecast at a  $1 \times 1$  km resolution.

In Figure 5, rank histograms for the predictions of the time to hard freeze are presented. They show that, on average over all study locations, the raw ensemble tends to overestimate the time to hard freeze. However, the histogram does not show any signs of under- or overdispersion. Figure 5 further shows that the rank histogram for the post-processed forecasts appears uniform indicating an overall calibrated forecast. Hence, the post-processing of the  $1 \times 1^\circ$  daily temperature forecasts also results in well-calibrated

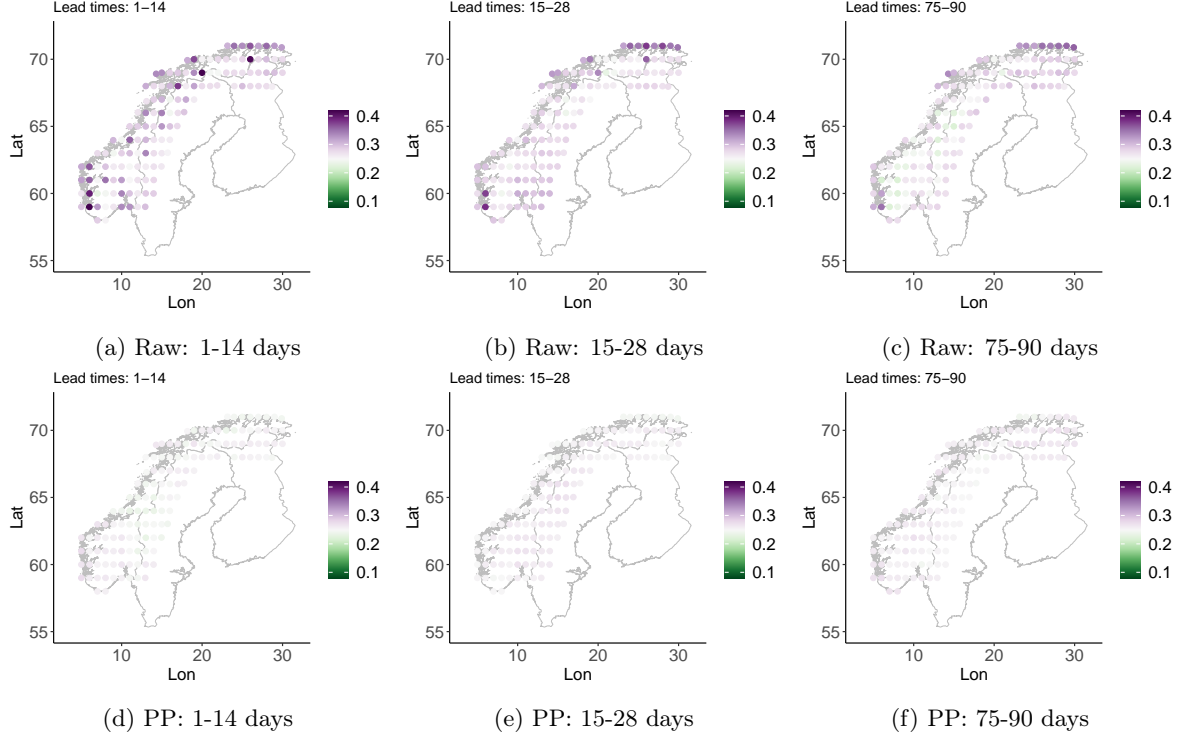


Figure 4: Absolute deviance from 0.5 of observed standardized ranks for each location for daily temperature forecasts initialized on October 1 aggregated over 1993-2020, for daily lead times 1-14 (leftmost column), 15-28 (middle column) and 75-90 (rightmost column), for the raw (top row) and the postprocessed ensemble (bottom row). For a calibrated forecast, the mean absolute deviance should be 0.25.

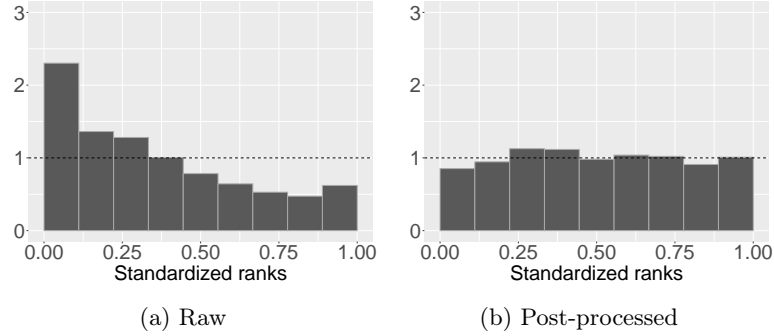


Figure 5: Rank histograms for the time to hard freeze forecasts for the raw (left) and the postprocessed ensemble (right) initialized on October 1, aggregated over the years 1993-2020 and the study locations shown in Figure 1.

predictions for the time to hard freeze for our study locations.

## 5.2 Evaluation of the time to hard freeze forecasts

### 5.2.1 Overall performance

In this section, we evaluate the overall performance of the proposed time to hard freeze KM forecasts. In Figure 6, the integrated Brier skill scores for all study locations are presented, both for the raw forecast  $\hat{S}_{sy}^R(t)$  and the post-processed forecast  $\hat{S}_{sy}^P(t)$ , where they are compared against climatology. The results show that  $\hat{S}_{sy}^R(t)$  yields negative skill scores at many grid points, particularly in coastal areas, while in regions far away from the coast, the skill score is positive. In coastal areas, the frost in general comes later than in nearby non-coastal areas and is thus more difficult to predict with the October 1 initialization. The low spatial resolution of the forecasts can also be particularly challenging here, and is likely responsible for some of the biases noted above, especially as grid cells close to the coast overlap partially sea and

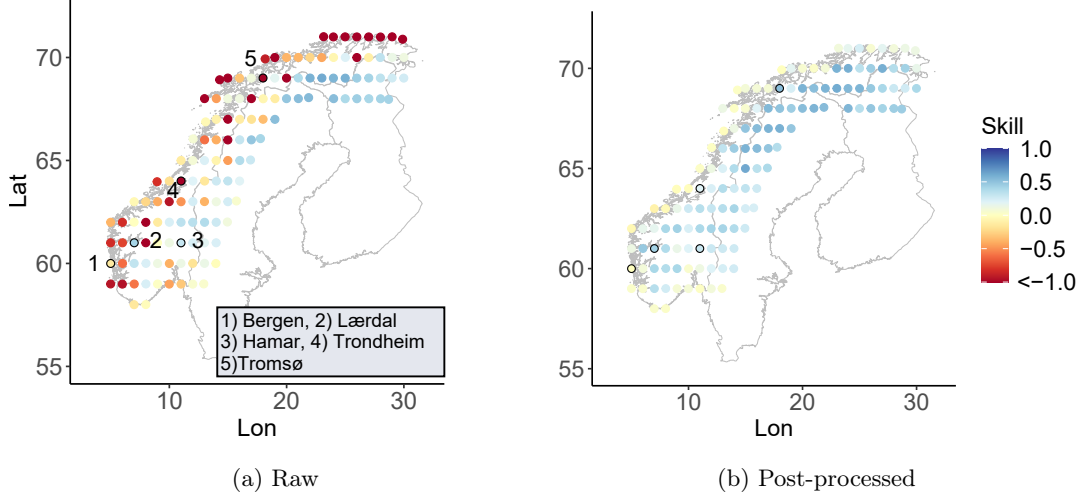


Figure 6: Integrated Brier skill scores for time to hard freeze forecasts initialized on October 1 aggregated over 1993-2020 for the raw temperature forecasts  $\hat{S}^R(t)$  and the post-processed temperature forecasts  $\hat{S}^P(t)$  relative to the climatological forecast  $\hat{S}^C(t)$ . Five locations, close to the Norwegian cities/towns Bergen, Lærdal, Hamar, Trondheim and Tromsø, are marked with black circles for further reference. See also Table 2.

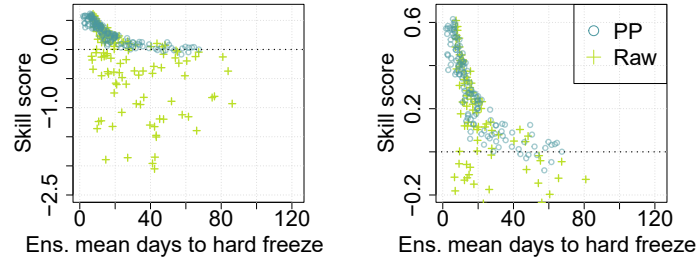
partially land. This may be intensified by the fact that we have combined NWP products from different spatial grids. Furthermore, the west coast of Norway is quite mountainous, yielding rapidly changing temperatures fields.

Figure 6b shows that the post-processing procedure increases the skill in areas where  $\hat{S}_{sy}^R(t)$  performed poorly. The post-processed model  $\hat{S}_{sy}^P(t)$  yields positive skill scores at most study locations, with near-zero skill scores near the coast. Consequently, the post-processed model performs just as well as a climatology forecast in coastal regions, and consistently outperforms climatology at most grid points.

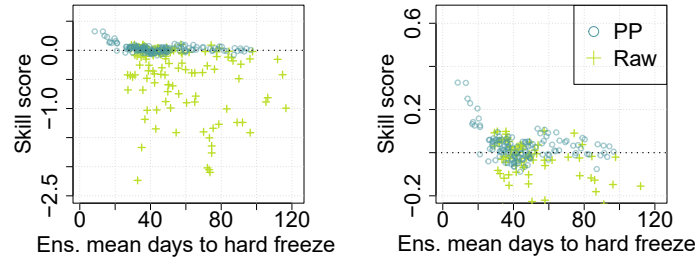
Figure 7a presents the skill score for each of the 135 study locations as a function of the mean predicted days to hard freeze from October 1. Here, the mean predicted days to hard freeze are obtained from the historical ensemble means for 1993-2020 for the raw or the post-processed ensemble, respectively. The figure shows that the skill score of the post-processed forecasts is positive for almost all study locations and that all locations where the average predicted time to hard freeze is less than 40 days have a positive skill score. The skill of the forecasts decrease with increasing mean predicted time to hard freeze, as expected. However, for many of the locations where the mean predicted time to hard freeze is 15-30 days, the skill score is still quite high (0.10-0.20).

For reference, we also include the skill scores we obtain when we use forecasts with initialization date September 1 over the same period 1993-2020, see Figure 7b. The first occurrence of hard freeze from September 1 is usually further away from the initial date than for a counter that starts on October 1. However, the results from the September forecasts are comparable to the results from the October forecasts: For locations where hard freeze is expected within 30 days, the skill score tends to be positive and often high (0-0.35) for the post-processed forecasts. When the predicted time to hard freeze is more than 30 days, the quality of the forecasts is more variable with skill scores distributed around 0.

In Figures 8a-8c, we show the difference between the ensemble mean days to hard freeze for our post-processed ensemble and the historically observed mean days to hard freeze (1993-2020) for three selected years: 2005, 2006 and 2007. This is a way to illustrate whether the forecasts predict hard freeze to come earlier or later than usual in different parts of the country. For example in 2006, the NWP systems predicted the hard freeze to come later than usual in the southern parts of Norway and earlier than usual in the northern parts. In Figures 8d-8f, we visualize what actually happened in 2005-2007 by showing the difference between the observed days to hard freeze and the historically observed mean days to hard freeze (1993-2020). The figures of 2005 and 2006 reveal that while the forecasts were not able to exactly predict the number of days to hard freeze at every single location, they were able to capture the large, general trends. Fall 2005 was indeed warmer than usual for most locations, and in 2006 the hard freeze came late in southern Norway and early in northern Norway as predicted. There are also some years where the overall performance is not as good, as year 2007 show. Comparing skill scores over years shows



(a) Forecasts initialized on October 1



(b) Forecasts initialized on September 1

Figure 7: Top row: The location-specific skill scores in Figure 6 plotted as a function of the locations' mean predicted days to hard freeze. For the raw forecast, the mean predicted days are calculated from the raw ensemble mean for 1993-2020 (crosses), and for the post-processed forecast it is calculated from the post-processed ensemble mean (dots). The right plot is a zoomed-in version of the left plot. Bottom row: Corresponding results for forecasts initialized on September 1.

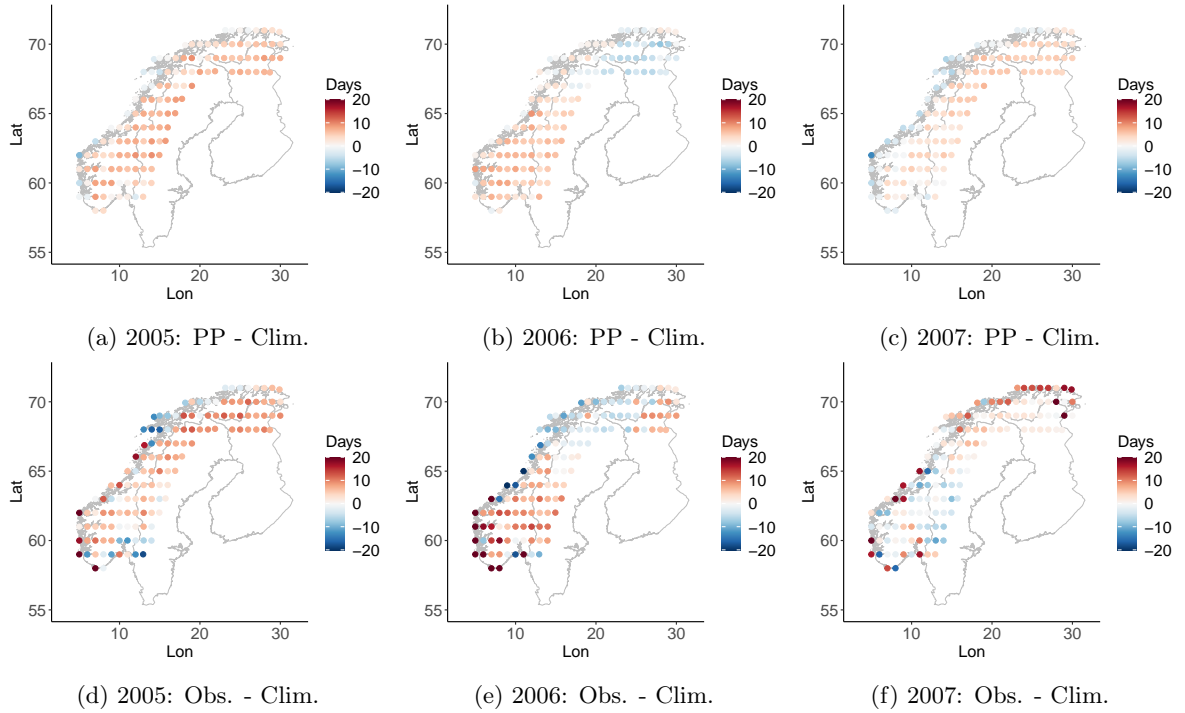


Figure 8: Top row: The deviation of the post-processed ensemble mean number of days to hard freeze in three given years from the climatological average over 1993-2020. Bottom row: Observed anomaly in days to hard freeze in the same three years. Positive values indicate that hard freeze was predicted or observed to come later than on average compared to the reference period.



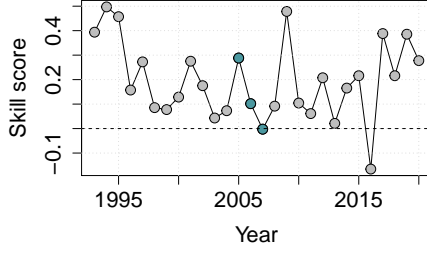


Figure 9: Year-specific skill scores for the post-processed forecast (1993-2020). The example years from Figure 8 are marked.

that 2007 is ranked as the year with the second lowest skill score for the post-processed forecast, with skill score 0. In comparison, the skill scores for years 2005 and 2006 are 0.29 and 0.11 respectively. See Figure 9 for skill scores as a function of year for the post-processed forecasts.

We find more years comparable to the 2005 and 2006 examples in our reference period 1993-2020. In the next subsection we will show some examples of how survival curves can be used as a tool to evaluate whether hard freeze comes early or late locally, in a more probabilistic manner.

### 5.2.2 Time to hard freeze forecasts at five selected locations

We now present example time to hard freeze forecasts for five locations in Norway expressed probabilistically through the KM estimator of the survival curve. The selected locations are close to Bergen, Hamar, Lærdal, Tromsø and Trondheim and are marked in Figure 6a. See Table 2 for more information about each location. We also refer to the files attached to the paper, where observations and forecasts for these five locations are included together with code for calculating and plotting the KM estimator for 1993-2020.

Table 2: Location characteristics and integrated Brier skill scores aggregated over 1993-2020 compared to climatology for the locations marked in Figure 6a. Mean dtf indicates the historical mean days to hard freeze from October 1 over 1993-2020, while sd dtf indicates the corresponding standard deviation based on the seNorge data product.

Location	Lon	Lat	seNorge elev. (m a.s.l.)	Mean dtf (days)	Sd dtf (days)	Skill $\hat{S}_{sy}^R(t)$	Skill $\hat{S}_{sy}^P(t)$
Trondheim	11	64	386	20	13	-1.19	0.20
Hamar	11	61	535	16	10	0.30	0.29
Bergen	5	60	0	71	18	-0.13	0.00
Lærdal	7	61	1050	10	9	0.42	0.43
Tromsø	18	69	391	8	6	-1.08	0.52

Figure 10 presents  $\hat{S}_{sy}^P(t)$ ,  $\hat{S}_{sy}^R(t)$  and  $\hat{S}_{sy}^C(t)$  for five example years for the location at longitude  $11^\circ$  and latitude  $64^\circ$ , near the Norwegian city Trondheim. This is a region with a high density of farms and where a hard freeze forecast could be useful. We see that  $\hat{S}_{sy}^P(t)$  has high skill, and performs considerably better than  $\hat{S}_{sy}^R(t)$ . According to Figure 10, the raw ensemble often overestimates the time to hard freeze by several weeks and gives an uncertainty that is too large. The forecasts given by the post-processed ensembles are sharper and for many of the study years they correspond quite well to what we observe: The probability that hard freeze has not occurred is often around 0.5 around the time when the first hard freeze actually arrived (dashed line). See years 2005, 2006, 2008 and 2009 in Figure 10. Also note how comparing  $\hat{S}_{sy}^P(t)$  and  $\hat{S}_{sy}^C(t)$  gives information on whether hard freeze can be expected to come earlier or later than usual. In 2009, for example, the post-processed survival curve in general drops faster than the climatological survival curve, suggesting that hard freeze can be expected earlier than usual. This was also what actually happened this year. The last panel in Figure 10 reveals that  $\hat{S}_{sy}^P(t)$  gave the best forecast for 17 out of 28 study years. The overall skill scores for  $\hat{S}_{sy}^R(t)$  and  $\hat{S}_{sy}^P(t)$  are -1.19 and 0.20 respectively, as summarized in Table 2.

We next consider survival curves for the location in the Hamar area, at longitude  $11^\circ$  and latitude  $61^\circ$ , see Figure 11. The Hamar region is another area of Norway where we find many farms and where a forecast



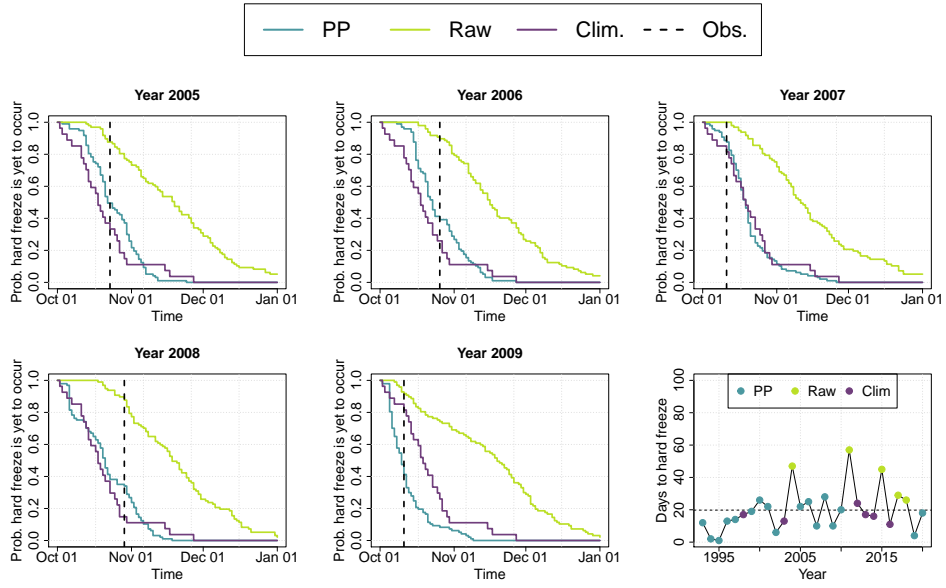


Figure 10: Survival curves for days to hard freeze based on the KM estimator for five selected years at a location close to Trondheim, at longitude  $11^\circ$  and latitude  $64^\circ$ , with the observed first day of hard freeze indicated with a dashed line. The lower rightmost plot shows the observed number of days to hard freeze for all years in the study period with each observation colored according to the forecast that performed best in that year based on the integrated Brier score.

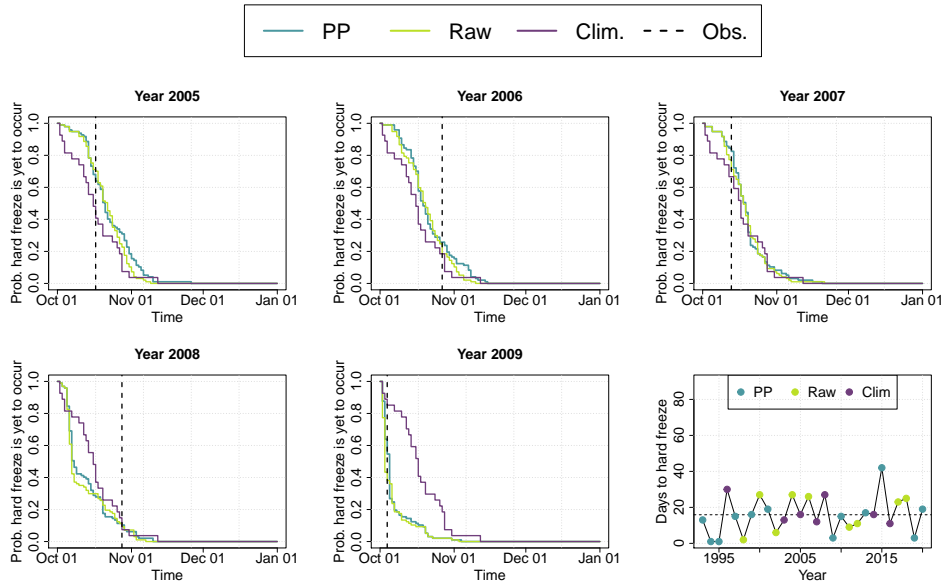


Figure 11: As Figure 10, but for a location in the Hamar area, at longitude  $11^\circ$  and latitude  $61^\circ$ .

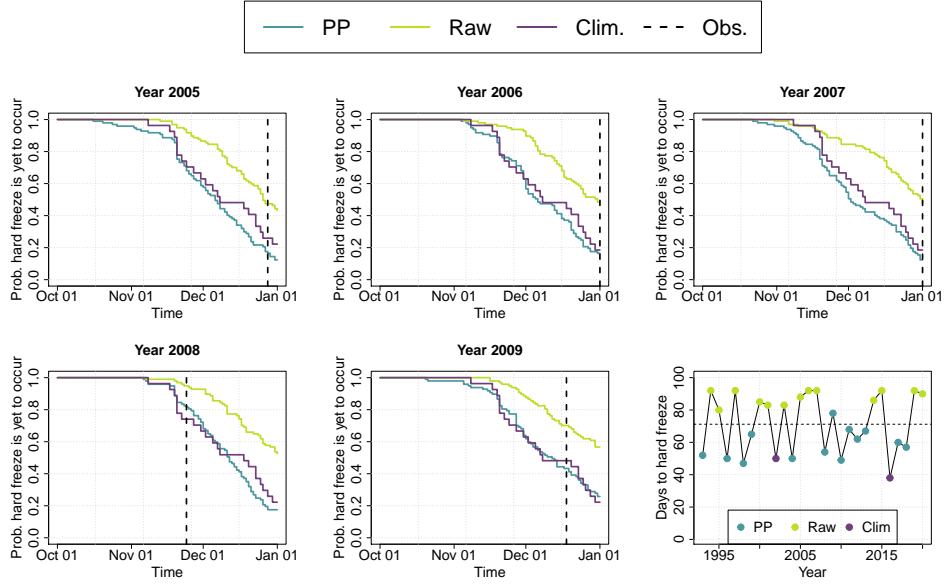


Figure 12: As Figure 10, but for a location south of Bergen, at longitude  $5^\circ$  and latitude  $60^\circ$ .

for the days to hard freeze could be valuable. The hard freeze comes 16 days after October 1st on average according to the seNorge data product. We see that  $\hat{S}_{sy}^P(t)$  and  $\hat{S}_{sy}^R(t)$  give more similar forecasts here compared to what we saw for Trondheim. Both  $\hat{S}_{sy}^P(t)$  and  $\hat{S}_{sy}^R(t)$  seem to capture the probability of hard freeze occurrence quite well, with probabilities around 0.5 in the time periods where hard freeze occurred historically. This can e.g. be seen for years 2005, 2007 and 2009 in Figure 11. According to Table 2, the overall skill scores of  $\hat{S}_{sy}^P(t)$  and  $\hat{S}_{sy}^R(t)$  are 0.29 and 0.30 respectively. We see similar trends as in Hamar for many of the locations in the interior parts of southern Norway and Sweden. The year-to-year variability in the number of days to hard freeze is in general low (Figure 1b) and the forecast skill is high (Figure 6).

Figure 12 presents the survival curves for a location where the forecasts are less skillful. The selected location is at longitude  $5^\circ$  and latitude  $60^\circ$ , which is on the west coast of Norway, south of Bergen. The mean number of days to hard freeze, from October 1, is 71 days, and Figure 12 shows that the variability in the predicted time to hard freeze is also large. The shapes of  $\hat{S}_{sy}^P(t)$  and  $\hat{S}_{sy}^R(t)$  tell us that the next hard freeze can come almost any time between day 14 and day 92 for some of the example years. The number of days to hard freeze varies a lot historically too, which we see from the shape of the baseline model  $\hat{S}_{sy}^C(t)$ . For some of the historical years, hard freeze is not observed before the end of our study period on December 31. In general,  $\hat{S}_{sy}^R(t)$  predicts that hard freeze comes later than  $\hat{S}_{sy}^C(t)$ . The overall skill scores of  $\hat{S}_{sy}^R(t)$  and  $\hat{S}_{sy}^P(t)$  are -0.13 and 0.00 respectively (Table 2), which means that  $\hat{S}_{sy}^P(t)$  on average is approximately as accurate as the climatological model  $\hat{S}_{sy}^C(t)$ . We see large deviance between the raw and post-processed forecasts for many of the locations along the Norwegian coast. Further investigation reveals that the raw forecast can both under- and overestimate the time to hard freeze. This was also indicated by the results for the daily temperature forecasts shown in Figure 3.

In Figure 13, survival curves for the Tromsø and Lærdal area are presented. Tromsø is located far north in Norway, while the location close to Lærdal is in the interior of southern Norway, at elevation 1050 m a.s.l. The skill of the post-processed forecast  $\hat{S}_{sy}^P(t)$  is high for both locations, with skill scores 0.52 and 0.43, respectively. Most years,  $\hat{S}_{sy}^C(t)$  and/or  $\hat{S}_{sy}^P(t)$  have probabilities around 0.5 around the time when the first hard freeze after October 1 was observed. The forecasts also often correctly identify whether the hard freeze comes earlier or later than usual. See e.g.  $\hat{S}_{sy}^P(t)$  for Tromsø in 2005 and for Lærdal in 2006.

The high skill for Lærdal and Tromsø can be explained by the early hard freeze, on average 8-10 days after October 1. In some years, hard freeze has already occurred by the initialization date. This happens in Tromsø in 2006 and 2008, and at Lærdal in 2008 (Figure 13). The trends we see for Tromsø and Lærdal can also be seen for other locations north in the study area and in the mountainous areas in southern Norway. A difference between Tromsø and Lærdal is that for Lærdal, the raw forecast performs approximately as well as the post-processed forecast, see Table 2. Around Tromsø, the raw forecast gives

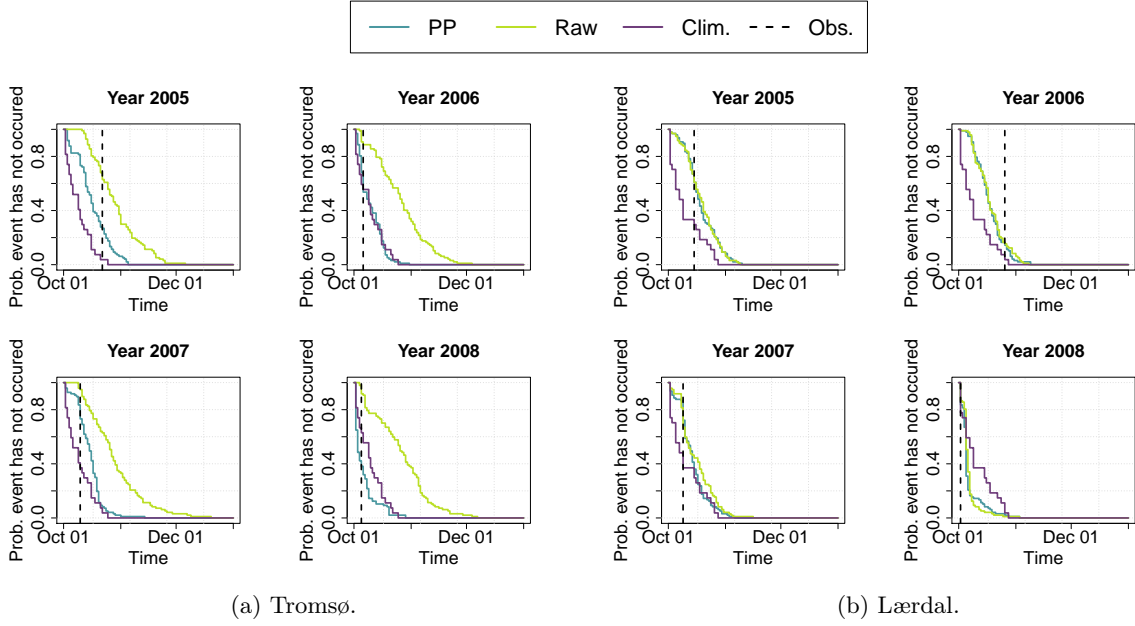


Figure 13: As Figure 10, but for a location in the Tromsø area (longitude  $18^\circ$ , latitude  $69^\circ$ ) and close to Lærdal (longitude  $7^\circ$ , latitude  $61^\circ$ ).

an overall skill score around -1. This can be explained by that Tromsø is close to the coast. In coastal areas the skill of the raw forecast is poor in general as Figure 6a shows. The results for  $\hat{S}_{sy}^P(t)$  for Tromsø (and also for e.g. Bergen and Trondheim) however illustrates that the post-processing algorithm is able to adjust the coarse NWP forecasts such that they become skillful locally.

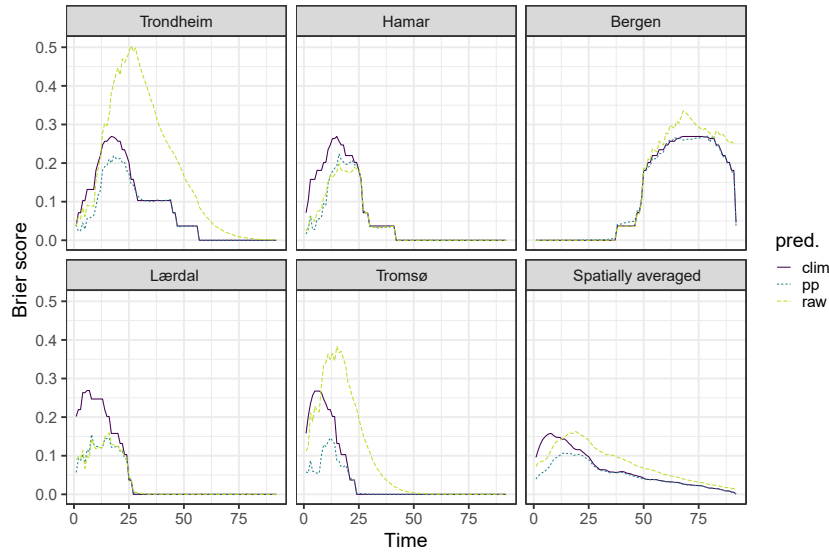


Figure 14: Mean Brier scores over the study period 1993-2020 at the five example locations indicated in Figure 6a and spatially averaged over all study locations, given as functions of lead time for the three time to freeze forecasts initialized on October 1.

While the skill scores considered in Section 5.2.1 assess the overall fit of the predicted time to hard freeze, we can gain some insights into how the error varies with the prediction time horizon by plotting the average Brier score  $BS(t)$  as a function of  $t$ . Figure 14 shows the Brier scores for the five example locations considered in this Section, as well as  $BS(t)$  averaged across all considered grid points shown in Figure 1.

The post-processed predictions consistently perform best across all examples and lead times, with near-climatological skill at long lead times. This is quite remarkable, since the post-processing technique is

rather simple and was applied to surface temperature forecasts, not to the prediction target, i.e. the time to hard freeze. At first glance, it might seem counter-intuitive that the prediction error decreases after a certain lead time. However this is simply due to the fact that we predict whether hard freeze has occurred at any time up to time  $t$ , not whether it occurred at time  $t$ . At long lead times the score converges to zero, because the climatological uncertainty of the predicted event goes to zero, which can be formalized by the score decompositions used in Murphy and Winkler (1987) and Bröcker (2009). In particular, the time horizon when the score of the climatological model drops to zero highlights the latest occurrence of the first hard freeze present in our data at that location. For Bergen, the climatological model has a Brier score of 0 up to  $t = 38$ , highlighting that hard freeze never occurred before this time in our data.

## 6 Discussion

In this paper we propose to use techniques from survival analysis in combination with long-range numerical weather predictions to generate probabilistic forecasts for the time to the next hard freeze from an initialization date. The forecasts were evaluated for a region in Fennoscandia that covers Norway and parts of Sweden, Finland and Russia. The time to the next hard freeze is an example of an agroclimatic indicator that is highly relevant for agricultural operations planning. However, it cannot be derived from currently available seasonal forecast products which typically come in the form of averages over one or several months. This kind of aggregation is usually necessary for predictions to be skillful at a seasonal time scale. A priori, it is thus not clear whether model output from long-range NWP systems contains information that can be used to make skillful prediction of agroclimatic indicators like the time to the first hard freeze. The results presented in Section 5 suggest that at locations where the climatological average time to the first hard freeze is less than 40 days, skillful probabilistic predictions can indeed be obtained with our framework of post-processed, multi-model ensemble weather predictions.

The current time to hard freeze predictions are just one example of a wide range of meteorological time-to-event indicators that may fit well within the general survival time analysis framework. Other examples include the time to next drought, the time to the onset of the rain season, or the time to the next sudden stratospheric warming. Here, the general idea is to treat each ensemble member as one would treat an individual in a classical survival analysis setting. As far as the authors know, this is a new way to apply survival time models. Output from several NWPs can be combined to achieve a sufficiently large sample size for statistical analyses at separate locations. The survival curve examples in Section 5 illustrate how the shape of the survival function provide an intuitive way of presenting the uncertainty of a time-to-event forecast and the probability of an event occurring earlier or later than usual.

Now that the applicability of survival models in long range weather forecasting is demonstrated, there exists a large collection of methods that can be used to build more advanced models for the time to hard freeze or other meteorological events of interest. A natural extension of the hard freeze analysis, is to replace the non-parametric KM estimator by a parametric or semi-parametric survival function. This can be achieved by using a proportional hazards model. In a proportional hazards model, the time to an event  $t$  is modeled through a hazard rate  $h(t)$  that expresses the probability of experiencing the event during the next instant of time after time  $t$ , given that the event has not already occurred. The hazard rate is given as a function of explanatory variables that are multiplicative with respect to a baseline hazard function  $h_0(t)$ , for example as  $h(t|\mathbf{x}_i) = h_0(t) \times \exp(b_1x_{i1} + \dots + b_px_{ip})$ , where  $\mathbf{x}_i = (x_{i1}, \dots, x_{ip})$  is a vector of  $p$  covariates associated with individual (or ensemble member)  $i$ , and  $h_0(t)$  is a parametric or non-parametric model. The above form of  $h(t|\mathbf{x}_i)$  is known as a Cox proportional hazards model (Cox, 1972) and has been used in a variety of applications (e.g. Lane et al., 1986; Kumar and Klefsjö, 1994).

In a hard freeze forecasting context, a proportional hazard model can be applied to build a joint model for all study locations using explanatory variables like longitude, latitude and elevation. From the parametric relationship, predictions for any location can be derived. If we want to take the model a step further, one could add random effects to the exponential part of  $h(t|\mathbf{x}_i)$ , e.g. a Gaussian random field that captures spatial and/or temporal correlation (Martino et al., 2011; Aswi et al., 2020; Zhou et al., 2020; Gómez-Rubio, 2020). A fundamental assumption in the proportional hazard model is that the hazard ratio of two individuals is independent over time. If this is inappropriate, one can consider a Cox model with time dependent regression coefficients (Ata Tutkun and Tekin, 2007) or an accelerated failure time model that assumes that the effect of a covariate increases or decreases during the study period by some constant (Faruk, 2018; J., 1992). There also exist survival models where the hazard rate is estimated by using neural networks or other machine learning techniques (Faraggi and Simon, 1995; Katzman et al., 2018).

In the hard freeze study, we use the ensemble members from long-range NWP systems as input to our survival model. These were easily accessible and provided around 100 ensemble members per location and year. A disadvantage with using the CDS seasonal forecasts, is that they are only produced once a month and published around 12 days after their initialization date. This makes it challenging to operationalize the forecast, particularly as our results indicate that the forecasts mainly have high skill in areas where the first hard freeze comes less than 4 weeks after the initialization date. As an alternative to the seasonal forecasts, one could use subseasonal forecasts, e.g. the extended-range forecasts from ECMWF that have lead time 0-46 days and are published twice a week. The drawback is that their hindcasts only have 11 ensemble members, which hampers model validation. Furthermore, with a maximum lead time of 46 days we also lose the opportunity to study the future daily temperature to a point where it has dropped to zero at almost every location in Norway. The last is feasible with the seasonal forecasts with initialization date of September 1 or October 1.

The overlapping release of forecast products, the varying length of their lead times, and the often substantially different ensemble sizes of each product poses a critical operational challenge in general, and for hard freeze modeling in particular. Substantial effort will now be placed on the problem of data fusion, where a long-range forecast is updated on a daily basis to incorporate new observations and new forecasts across all time scales. One of the motivating reasons for choosing the survival time framework was that it is highly amenable to incorporate these concepts. In the future, we envision a system which dynamically updates survival time forecasts on the basis of observations and updates to forecasting systems.

When making forecasts for the agricultural sector, it is important to also consider the most reasonable definition of the relevant meteorological event for the particular application. In the case of hard freeze, the definition should depend on the type of crop we are interested in and the temperatures that are harmful for that specific culture. Potatoes protected by the soil can e.g. handle a lower temperature than berries or fruit. For some crops it might be the minimum temperature during a day that matters, while for others it could be the mean temperature over several days. Luckily, any such definition fits into the survival time framework outlined in this paper. The models can also easily be rephrased to consider the time to the last hard freeze or frost before spring.

## Acknowledgements

The authors thank Ellen-Margrethe Hovland, Trine Thanh Ha and Stian Bjørntvedt for helpful discussions. This work was supported by the Research Council of Norway through grants 309562 "Climate Futures" and 270733 "Seasonal Forecasting Engine".

## References

- D.-A. An-Vo, S. Mushtaq, K. Reardon-Smith, L. Kouadio, S. Attard, D. Cobon, and R. Stone. Value of seasonal forecasting for sugarcane farm irrigation planning. *European journal of agronomy*, 104:37–48, 2019.
- J. R. Angel, M. Widhalm, D. Todey, R. Massey, and L. Biehl. The U2U corn growing degree day tool: Tracking corn growth across the US Corn Belt. *Climate Risk Management*, 15:73–81, 2017.
- A. Aswi, S. Cramb, E. Duncan, W. Hu, G. White, and K. Mengersen. Bayesian spatial survival models for hospitalisation of dengue: A case study of wahidin hospital in makassar, indonesia. *International Journal of Environmental Research and Public Health*, 17(3), 2020. ISSN 1660-4601. doi: 10.3390/ijerph17030878.
- N. Ata Tutkun and M. Tekin. Cox regression models with nonproportional hazards applied to lung cancer survival data. *Haceteppe Journal of Mathematics and Statistics*, 36:157–167, 01 2007.
- D. Belušić, H. de Vries, A. Dobler, O. Landgren, P. Lind, D. Lindstedt, R. A. Pedersen, J. C. Sánchez-Perrino, E. Toivonen, B. van Ulft, F. Wang, U. Andrae, Y. Batrak, E. Kjellström, G. Lenderink, G. Nikulin, J.-P. Pietikäinen, E. Rodríguez-Camino, P. Samuelsson, E. van Meijgaard, and M. Wu. Hclim38: a flexible regional climate model applicable for different climate zones from coarse to convection-permitting scales. *Geoscientific Model Development*, 13(3):1311–1333, 2020. doi: 10.5194/gmd-13-1311-2020.
- G. W. Brier. Verification of forecasts expressed in terms of probability. *Monthly weather review*, 78(1):1–3, 1950.
- J. Bröcker. Reliability, sufficiency, and the decomposition of proper scores. *Quarterly Journal of the Royal Meteorological Society*, 135(643):1512–1519, 2009.
- D. R. Cox. Regression models and life-tables. *Journal of the Royal Statistical Society: Series B (Methodological)*, 34(2): 187–202, 1972. doi: 10.1111/j.2517-6161.1972.tb00899.x.

- M. Dabernig, G. Mayr, J. Messner, and A. Zeileis. Spatial ensemble post-processing with standardized anomalies. Quarterly Journal of the Royal Meteorological Society, 143:909–916, 2017.
- H. B. Erlandsen, S. Beldring, S. Eisner, H. Hisdal, S. Huang, and L. M. Tallaksen. Constraining the HBV model for robust water balance assessments in a cold climate. Hydrology Research, 52(2):356–372, 01 2021. ISSN 0029-1277. doi: 10.2166/nh.2021.132.
- D. Faraggi and R. Simon. A neural network model for survival data. Statistics in Medicine, 14(1):73–82, 1995. doi: 10.1002/sim.4780140108.
- A. Faruk. The comparison of proportional hazards and accelerated failure time models in analyzing the first birth interval survival data. Journal of Physics: Conference Series, 974:012008, 03 2018. doi: 10.1088/1742-6596/974/1/012008.
- R. Fischer and D. Connor. Issues for cropping and agricultural science in the next 20 years. Field Crops Research, 222: 121–142, 2018.
- L. Gandin and R. Hardin. Objective analysis of meteorological fields. Israel program for scientific translations, Jerusalem, 242, 1965.
- H. R. Glahn and D. A. Lowry. The use of model output statistics (MOS) in objective weather forecasting. Journal of Applied Meteorology, 11:1203–1211, 1972.
- V. Gómez-Rubio. Bayesian inference with inla. Chapman & Hall/CRC Press, Boca Raton, FL, 2020.
- T. Gneiting, A. E. Raftery, A. H. Westveld, and T. Goldman. Calibrated probabilistic forecasting using ensemble model output statistics and minimum crps estimation. Monthly Weather Review, 133:1098–1118, 2005.
- T. Gneiting, F. Balabdaoui, and A. E. Raftery. Probabilistic forecasts, calibration and sharpness. Journal of the Royal Statistical Society: Series B (Statistical Methodology), 69(2):243–268, 2007.
- T. M. Hamill. Interpretation of rank histograms for verifying ensemble forecasts. Monthly Weather Review, 129(3):550–560, 2001.
- G. Hammer, D. Holzworth, and R. Stone. The value of skill in seasonal climate forecasting to wheat crop management in a region with high climatic variability. Australian Journal of Agricultural Research, 47(5):717–737, 1996.
- K. Handeland, K. Tunheim, K. Madslie, T. Vikøren, H. Viljugrein, A. Mossing, I. Børve, O. Strand, and I. S. Hammes. High winter loads of Oestrid larvae and *Elaphostomum* Rangiferi are associated with emaciation in wild reindeer calves. International Journal for Parasitology: Parasites and Wildlife, 15:214–224, 2021. ISSN 2213-2244. doi: 10.1016/j.ijppaw.2021.05.008.
- C. Heinrich. On the number of bins in a rank histogram. Quarterly Journal of the Royal Meteorological Society, 147(734): 544–556, 2021.
- C. Heinrich, K. H. Hellton, A. Lenkoski, and T. L. Thorarindottir. Multivariate postprocessing methods for high-dimensional seasonal weather forecasts. Journal of the American Statistical Association, 116(535):1048–1059, 2021.
- S. Hemri, M. Scheuerer, F. Pappenberger, K. Bogner, and T. Haiden. Trends in the predictive performance of raw ensemble weather forecasts. Geophysical Research Letters, 41:9197–9205, 2014.
- S. Hemri, J. Bhend, M. A. Liniger, R. Manzanar, S. Siegert, D. B. Stephenson, J. M. Gutiérrez, A. Brookshaw, and F. J. Doblas-Reyes. How to create an operational multi-model of seasonal forecasts? Climate Dynamics, 55(5):1141–1157, 2020.
- H. Hersbach. Decomposition of the continuous ranked probability score for ensemble prediction systems. Weather and Forecasting, 15(5):559–570, 2000.
- W. L. J. The accelerated failure time model: a useful alternative to the Cox regression model in survival analysis. Statistics in medicine, 11 (14-15):1871–1879, 1992. doi: 10.1002/sim.4780111409.
- J. D. Kalbfleisch and R. L. Prentice. The statistical analysis of failure time data, volume 360. John Wiley & Sons, 2011.
- E. Kalnay. Atmospheric modeling, data assimilation and predictability. Cambridge university press, 2003.
- E. L. Kaplan and P. Meier. Nonparametric estimation from incomplete observations. Journal of the American statistical association, 53(282):457–481, 1958.
- J. L. Katzman, U. Shaham, A. Cloninger, J. Bates, T. Jiang, and Y. Kluger. DeepSurv: personalized treatment recommender system using a Cox proportional hazards deep neural network. BMC medical research methodology, 18(1):1–12, 2018.
- R. Keller, J. Rajczak, J. Bhend, C. Spirig, S. Hemri, M. A. Liniger, and H. Wernli. Seamless multimodel postprocessing for air temperature forecasts in complex topography. Weather and Forecasting, 36(3):1031 – 1042, 2021. doi: 10.1175/WAF-D-20-0141.1.
- T. Klemm and R. A. McPherson. The development of seasonal climate forecasting for agricultural producers. Agricultural and forest meteorology, 232:384–399, 2017.
- M. S. Kukul and S. Irmak. US agro-climate in 20th century: growing degree days, first and last frost, growing season length, and impacts on crop yields. Scientific reports, 8(1):1–14, 2018.
- D. Kumar and B. Klefsjö. Proportional hazards model: a review. Reliability Engineering & System Safety, 44(2):177–188, 1994. ISSN 0951-8320. doi: 10.1016/0951-8320(94)90010-8.

- K. E. Kunkel, D. R. Easterling, K. Hubbard, and K. Redmond. Temporal variations in frost-free season in the United States: 1895–2000. *Geophysical Research Letters*, 31(3), 2004.
- W. R. Lane, S. W. Looney, and J. W. Wansley. An application of the Cox proportional hazards model to bank failure. *Journal of Banking & Finance*, 10(4):511–531, 1986. ISSN 0378-4266. doi: 10.1016/S0378-4266(86)80003-6.
- D. Lawrence. Uncertainty introduced by flood frequency analysis in projections for changes in flood magnitudes under a future climate in Norway. *Journal of Hydrology: Regional Studies*, 28:100675, 04 2020. doi: 10.1016/j.ejrh.2020.100675.
- J. Lehmann, M. Kretschmer, B. Schauburger, and F. Wechsung. Potential for early forecast of Moroccan wheat yields based on climatic drivers. *Geophysical Research Letters*, 47(12):e2020GL087516, 2020.
- S. Lerch, S. Baran, A. Möller, J. Groß, R. Scheffzik, S. Hemri, and M. Graeter. Simulation-based comparison of multivariate ensemble post-processing methods. *Nonlinear Processes in Geophysics*, 27(2):349–371, 2020. doi: 10.5194/npg-27-349-2020.
- B. Liu, M. Henderson, and M. Xu. Spatiotemporal change in China’s frost days and frost-free season, 1955–2000. *Journal of Geophysical Research: Atmospheres*, 113(D12), 2008.
- C. Lussana, O. Tveito, and F. Uboldi. Three-dimensional spatial interpolation of two-meter temperature over Norway. *Quarterly Journal of the Royal Meteorological Society*, 144, 01 2018. doi: 10.1002/qj.3208.
- C. Lussana, O. E. Tveito, A. Dobler, and K. Tunheim. seNorge \_2018, daily precipitation, and temperature datasets over Norway. *Earth System Science Data*, 11(4):1531–1551, 2019. doi: 10.5194/essd-11-1531-2019.
- S. Martino, R. Akerkar, and H. Rue. Approximate Bayesian inference for survival models. *Scandinavian Journal of Statistics*, 38(3):514–528, 2011. ISSN 03036898, 14679469.
- J. W. Messner, G. J. Mayr, and A. Zeileis. Nonhomogeneous boosting for predictor selection in ensemble postprocessing. *Monthly Weather Review*, 145(1):137 – 147, 2017. doi: 10.1175/MWR-D-16-0088.1.
- U. B. Mogensen, H. Ishwaran, and T. A. Gerds. Evaluating random forests for survival analysis using prediction error curves. *Journal of statistical software*, 50(11):1, 2012.
- A. H. Murphy and R. L. Winkler. A general framework for forecast verification. *Monthly weather review*, 115(7):1330–1338, 1987.
- S. Rasp and S. Lerch. Neural networks for postprocessing ensemble weather forecasts. *Monthly Weather Review*, 146(11):3885–3900, 2018.
- A. Robertson and F. Vitart. *Sub-seasonal to seasonal prediction: The gap between weather and climate forecasting*. Elsevier, 2018.
- P. J. Roebber and J. Crockett. Using a coevolutionary postprocessor to improve skill for both forecasts of surface temperature and nowcasts of convection occurrence. *Monthly Weather Review*, 147(11):4241 – 4259, 2019. doi: 10.1175/MWR-D-19-0063.1.
- M. D. Schwartz, R. Ahas, and A. Aasa. Onset of spring starting earlier across the Northern Hemisphere. *Global Change Biology*, 12(2):343–351, 2006.
- M. Taillardat, O. Mestre, M. Zamo, and P. Naveau. Calibrated ensemble forecasts using quantile regression forests and ensemble model output statistics. *Monthly Weather Review*, 144:2375–2393, 2016.
- B. Van Schaeybroeck and S. Vannitsem. Ensemble post-processing using member-by-member approaches: Theoretical aspects. *Quarterly Journal of the Royal Meteorological Society*, 141:807–818, 2015.
- B. Van Schaeybroeck and S. Vannitsem. Postprocessing of long-range forecasts. In *Statistical Postprocessing of Ensemble Forecasts*, pages 267–290. Elsevier, 2018.
- C. van Straaten, K. Whan, D. Coumou, B. van den Hurk, and M. Schmeits. The influence of aggregation and statistical post-processing on the subseasonal predictability of European temperatures. *Quarterly Journal of the Royal Meteorological Society*, 146(731):2654–2670, 2020.
- A. P. Weigel, M. A. Liniger, and C. Appenzeller. Seasonal ensemble forecasts: Are recalibrated single models better than multimodels? *Monthly Weather Review*, 137(4):1460–1479, 2009.
- J. F. Weltzin, J. L. Betancourt, B. I. Cook, T. M. Crimmins, C. A. Enquist, M. D. Gerst, J. E. Gross, G. M. Henebry, R. A. Hufft, M. A. Kenney, et al. Seasonality of biological and physical systems as indicators of climatic variation and change. *Climatic Change*, 163(4):1755–1771, 2020.
- D. S. Wilks. *Statistical methods in the atmospheric sciences*, volume 100. Academic press, 2011.
- F. Woldemeskel, D. McInerney, J. Lerat, M. Thyer, D. Kavetski, D. Shin, N. Tuteja, and G. Kuczera. Evaluating post-processing approaches for monthly and seasonal streamflow forecasts. *Hydrology and Earth System Sciences*, 22(12):6257–6278, 2018.
- D. Zhang, W. Xu, J. Li, Z. Cai, and D. An. Frost-free season lengthening and its potential cause in the Tibetan Plateau from 1960 to 2010. *Theoretical and applied climatology*, 115(3):441–450, 2014.
- H. Zhou, T. Hanson, and J. Zhang. spBayesSurv: Fitting Bayesian Spatial Survival Models Using R. *Journal of Statistical Software*, 92(9):1–33, 2020. doi: 10.18637/jss.v092.i09.